Optics Letters

Pump-power-controlled L-band wavelength-tunable mode-locked fiber laser utilizing nonlinear polarization evolution in all-polarization-maintaining fibers

Guanyu Ye,[1,2] Bowen Liu,[1,2] Maolin Dai,[1,2] Yifan Ma,[1,2] Takuma Shirahata,[1,2] Shinji Yamashita,[1,2] and Sze Yun Set[1,2,*]

[1]Research Center for Advanced Science and Technology, The University of Tokyo, 4-6-1 Komaba, Meguro-ku, Tokyo 153-8904, Japan
[2]Department of Electrical Engineering and Information Systems, The University of Tokyo, Bunkyo-ku, Tokyo 113-8656, Japan
*set@cntp.t.u-tokyo.ac.jp

Received 15 January 2024; revised 22 February 2024; accepted 15 March 2024; posted 15 March 2024; published 29 April 2024

We present for the first time, to the best of our knowledge, the pump-power-controlled, all-polarization-maintaining (all-PM), all-fiber configured, wavelength-tunable mode-locked fiber laser in the L-band (1565 to 1625 nm). A tuning range over 20 nm (1568.2 to 1588.9 nm) is attained simply by varying the pump power between 45 and 115 mW. Our work represents the first demonstration of wavelength tuning in all-PM configured nonlinear polarization evolution (NPE) lasers. The non-mechanical and electrically controllable tuning method offers ease of use and cost efficiency within an advanced all-PM, all-fiber design, indicating promising adaptability to diverse wavelength bands.

https://doi.org/10.1364/OL.518882

Wavelength-tunable mode-locked fiber lasers (MLFLs) have attracted increasing attention, notably for their applications in various fields such as optical spectroscopy [1], bio-imaging [2], and optical sensing [3]. L-band (1565 to 1625 nm) tunable mode-locked lasers expand the communication capacity [4] and emerge as a valuable light source for optical coherence tomography [5] and Raman scattering microscopy [6]. Through the second harmonic generation, they can produce 800 nm pulses, providing a compact substitute for bulky tunable Ti:Sapphire lasers in microscopy [7,8]. Various approaches have been investigated to achieve wavelength-tunable mode-locking in the L-band, including spectrum filters [9], intracavity loss control [10], and intracavity birefringence control [11]. Additionally, a soliton self-frequency shift (SSFS) has also been utilized for wavelength tuning via the adjustment of the injected pulse energy [12]. However, the non-polarization maintaining (non-PM) configurations of these lasers render them susceptible to environmental perturbations. The use of a polarization controller (PC) in the laser cavity further compromises the repeatability and reliability, limiting real-world applications. To overcome these issues, recent work has employed an all-PM, all-fiber setup with a built-in fiber Lyot filter. Although this setup allows for temperature or strain-controlled wavelength tuning, the tuning range is limited to 7 nm in the L-band [13,14].

In those studies, the mechanical and thermal tuning approaches introduce complexity to the laser setup, while a pump-power-controlled method offers a simplified and efficient alternative, promising for high-speed wavelength tuning. In 2023, an all-PM configured figure-9 mode-locked laser with a tuning method of pump power control was reported [15], though the laser was limited to a 5 nm tuning range and included free-space optical components. As of now, there is no report of L-band tunable mode-locked lasers featuring both a wide tuning range, all-fiber, all-PM design and pump-power-controlled tuning mechanisms.

In this Letter, we report the first pump-power-controlled, L-band tunable MLFL in an all-PM, all-fiber configuration, achieving a wide tuning range of 20 nm from 1568.2 to 1588.9 nm by simply adjusting the pump power between 45 and 115 mW. The mode-locking mechanism is based on a nonlinear polarization evolution (NPE) within all-PM fibers (PMFs), where the light pulse's polarization state evolves as it moves through angle-spliced PMF segments [16]. To our knowledge, our work marks the first experimental demonstration of pump-power controlled tunable MLFL using NPE in all-PMFs. We believe our work holds significant promise for adaptation across various wavelength bands for diverse applications.

The experimental setup of our all-PM NPE MLFL is illustrated in Fig. 1, and all the fibers and components are the PM types. A fast-axis-blocked PM tap isolating wavelength-division multiplexing (PM-TIWDM) acts as a polarizer, a WDM, an isolator, and a 10% output coupler. A 1.4-m-length of the PM-EDF (Nufern ESF-7/125) is backward pumped by a 980 nm laser diode (LD) and serves as the gain medium. The remaining fibers within the laser cavity are PANDA PM fibers (Fujikura SM15-PS-U25A). A fast-axis-blocked PM circulator (PM-CIR) functions as both a polarizer and an isolator, ensuring unidirectional propagation of the laser in the clockwise direction. The NPE structure

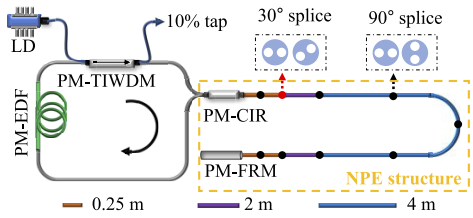

Fig. 1. Setup of the wavelength-tunable all-PM configured NPE MLFL. The PMF segment lengths are 0.25 m (orange), 2 m (purple), and 4 m (blue).

consists of a PM Faraday rotation mirror (PM-FRM), a PM-CIR, and a 21-m-length of PMF in between. The 21 m PMF within the NPE structure ensures an adequate modulation depth and suitably low saturation power for mode-locking [17].

The 21-m-length of the PMF comprises 10 segments, with the specific length of each segment in meters marked by different colors in Fig. 1. The angles at which each adjacent fiber segment is spliced vary as follows: there is one splicing angle of 30°, denoted in red, while the splicing angles for the remaining segments are all 90° (marked in black). The angle splicing is conducted using a splicer (Fujikura FSM-100P), ensuring that the loss at each splice point remains below 0.05 dB. The all-PM configured NPE lasers, with their angle splicing carefully managed, exhibit robust environmental stability [17,18]. The total cavity length is estimated to be 50 m, yielding a net group velocity dispersion of $-1.03\ \text{ps}^2$ at 1550 nm, which indicates the operation of the laser is in the soliton regime.

The NPE structure functions as an artificial saturable absorber (SA) [19]. The 30° angle splicing splits the linearly polarized light into two orthogonally polarized components along PMF principal axes, each with different pulse energies. Throughout the 21 m PMF round trip, pulse peaks and wings of both light components experience varied nonlinear phase shifts due to cross-phase modulation (XPM) and self-phase modulation (SPM), resulting in different nonlinear evolutions in polarization states. The PM-CIR, acting as a polarizer, applies a polarization-dependent loss—higher on pulse wings and lower at the peak—thereby enabling the NPE structure to function as an effective artificial SA for mode-locking. The FRM rotates the two light components' polarization by 90°, ensuring they travel an equal distance along each axis of the PMF during a complete round trip, thus offsetting the birefringence-induced walk-off [19].

The laser operates at room temperature without specific temperature or vibration control, with the 21 m PMF in the NPE section looped into circles of approximately 30 cm in diameter. The laser self-starts in a multi-pulse mode at a pump power of ~250 mW. Gradually lowering the pump power to ~115 mW induces a transition to a stable single-pulse operation, yielding an average output of ~80 μW at a central wavelength of 1588.9 nm. The multi-pulsing during self-starting, similar to that observed in the C-band PM NPE laser [20], may stem from the transmission characteristics of the reflected configured NPE artificial SA, which exhibits low nonlinear transmission at reduced pulse peak powers [19].

As the pump power decreases, the central wavelength blueshifts toward shorter values, reaching its shortest at 1568.22 nm at ~45 mW pump power. Figure 2 depicts the laser's performance at the initial and final points of the tuning range.

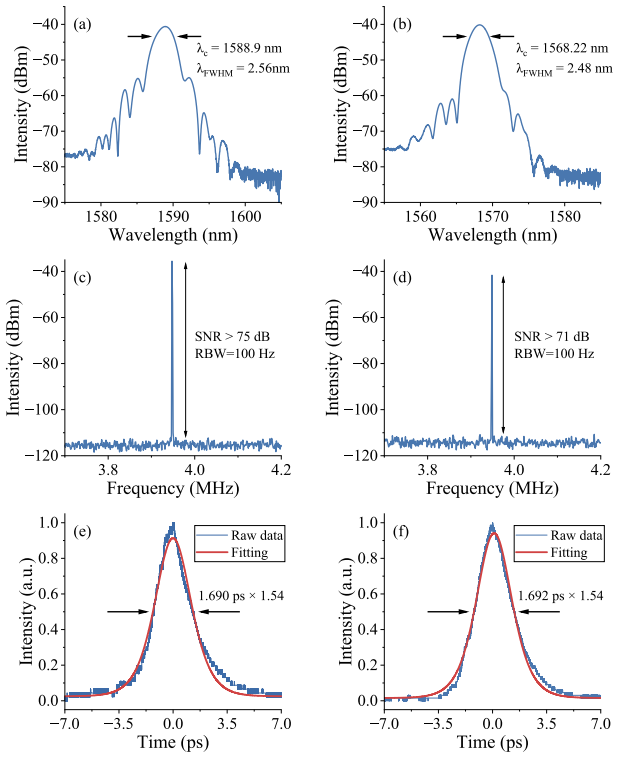

Fig. 2. Laser output characteristics: (a), (b) optical spectrum; (c), (d) RF spectrum (RBW, 100 Hz); (e), (f) AC trace (after 5 m PMF) at 1588.9 and 1568.2 nm, respectively.

The optical spectra, acquired by an optical spectrum analyzer (Yokogawa AQ6370D), are depicted in Figs. 2(a) and 2(b). The tuning range initiates at 1588.9 nm and concludes at 1568.2 nm, with a full-width-at-half-maximum (FWHM) spectrum bandwidth of 2.56 and 2.48 nm, respectively. The RF spectrum shown in Figs. 2(c) and 2(d), is measured with a photodetector (New Focus 1611) and an electrical spectrum analyzer (RIGOL RSA3045), confirming high pulse stability with signal-to-noise ratios (SNR) of 75 and 71 dB, respectively. The 3.9 MHz center frequency aligns with the ~50 m cavity length. The autocorrelation (AC) trace of the output pulse after a 5 m fiber pigtail is captured by directly recording the original output with an autocorrelator (Femtochrome FR 103XL) and an oscilloscope (RIGOL MSO8104), configured in an average mode with 16 times of averaging. Figures 2(e) and 2(f) show the estimated pulse widths of 1.69 ps at 1588.9 nm and 1.692 ps at 1568.2 nm, assuming a squared hyperbolic secant (sech^2) profile. Given the low pulse peak power, only the chromatic dispersion is considered for the output pulse propagation in the 5 m PMF pigtail. With a dispersion parameter of 23 ps/(nm·km) near 1.6 μm [21], the FWHM pulse width is estimated to broaden by 0.059 ps at 1588.9 nm and 0.057 ps at 1568.2 nm after 1 m of PMF propagation. Thus, intracavity FWHM pulse widths are estimated to be 1.395 ps at 1588.9 nm and 1.407 ps at 1568.2 nm, with time–bandwidth products of 0.424 and 0.425, respectively, indicating a slight chirp.

The L-band lasing is achieved through a gain profile shift using a longer PM-EDF and lower pump power [17,22]. Figure 3(a) presents the center wavelength tuning spectra, with the laser maintaining mode-locking across the 20 nm range. However, reducing the pump power below 40 mW leads to a loss

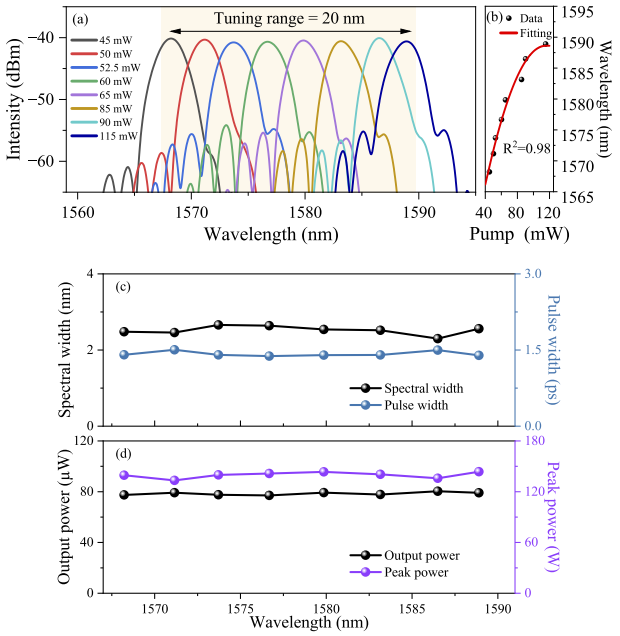

Fig. 3. Laser tuning performance. (a) Optical spectra at different pump powers; (b) center wavelength versus pump power; (c) FWHM spectral width and the corresponding pulse width; (d) output average power and intracavity peak power at different wavelengths.

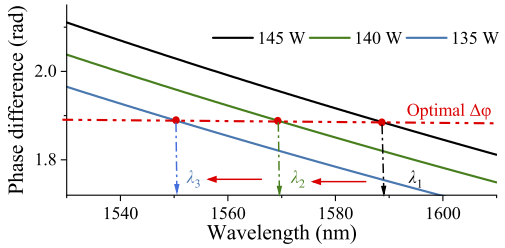

Fig. 4. Simulated overall phase difference at different pulse peak powers; the red dashed line marks the assumed optimal phase difference.

of mode-locking. Figure 3(b) illustrates a nonlinear relationship between the center wavelength and the pump power, as evidenced by a quadratic polynomial fitting with an R-square (R^2) of 0.98. This nonlinearity likely arises from variations in the gain profile at different pump powers. In the NPE mode-locking, the nonlinear phase accumulation depends on both the pulse peak power and the center wavelength. The change in pump power nonlinearly affects the pulse peak power, which in turn influences the center wavelength. Figure 3(c) displays FWHM spectral widths (2.3 to 2.66 nm) and pulse widths (1.38 to 1.5 ps) at different wavelengths. Given the minimal repetition rate variation (0.03%) across the 20 nm tuning range, we consider it constant for pulse power calculations. Figure 4(d) depicts the output average power and estimated intracavity peak powers, suggesting a relative stable pulse output with only a 1.4% standard deviation in average power throughout the tuning.

Our laser maintains mode-locking for a week at room temperature without special isolation, showing strong resilience to external disturbances. In the wavelength tuning repeatability tests, we consistently observed a stable 20 nm tuning range by pump power adjustment between ~45 and ~115 mW in each test, indicating the laser's robust reliability. Center wavelength variations, around 0.06 nm near 1589 nm and 0.4 nm near 1568 nm, likely stem from pump power instability at lower currents, suggesting potential improvements with more advanced laser drivers and pump lasers. The low output power and efficiency could be attributed to the EDF's limited gain in the L-band, a small output ratio, and high insertion loss of the CIR and FRM. Enhancing the output power and repetition rates can be achieved by minimizing intracavity losses, using couplers with higher output ratios and shortening the PMF in the NPE structure [23]. The tuning range could be broadened by optimizing EDF gain profiles [24], and the power stability is improved by shielding the laser from ambient temperature and vibration turbulence.

The pump-power-dependent wavelength tuning does not originate from the EDF gain curve shift, while the gain peak typically redshifts to longer wavelengths with decreasing pump power [25]. However, in our laser, the center wavelength experiences a blueshift to shorter values as the pump power reduces. Given this is the first demonstration of wavelength tuning in the all-PM configured NPE lasers, we present a plausible and reasonable theoretical explanation for the observed phenomena. The wavelength tuning is likely due to the mode-locking mechanism, which is the NPE in our laser. Wavelength tuning is characterized by a shift from mode-locking at one wavelength to another. This implies that both the original and new wavelengths meet the criteria for effective mode-locking by the NPE, which is based on the nonlinear evolution in the polarization state. Given that the evolution depends on the overall phase difference between the two orthogonal light components, it is suggested that a consistent or similar overall phase difference is maintained across both the original and new wavelengths. For a simplified analysis, we assume the overall phase difference between the two light components is preserved throughout the tuning process and focus on the center wavelength solely. The nonlinear phase shifts of the two polarized components, accumulated via XPM and SPM, are denoted as follows [20]:

$$\begin{aligned}\varphi_s &= \gamma L(|E_s|^2 + \frac{2}{3}|E_f|^2)\\ \varphi_f &= \gamma L(|E_f|^2 + \frac{2}{3}|E_s|^2),\end{aligned} \tag{1}$$

where, the nonlinear parameter $\gamma = 2\pi n_2/(\lambda A_{eff})$, n_2 is the nonlinear refractive index, and A_{eff} is the effective mode area. L represents the fiber length. E_s and E_f denote the electrical amplitudes of the light components along the slow and fast axes, respectively. The ratio of E_s to E_f is determined by the 30° angle splicing [26]. In our reflected all-PM NPE setup, both the two light components travel equal distances along the PMF axes, resulting in the same value of L and identical linear phase shifts for each component. Therefore, any difference in their overall phase is solely due to variations in the nonlinear phase shift. The overall phase difference can be expressed as

$$\Delta\varphi = \varphi_s - \varphi_f = \frac{2\pi L n_2}{3}\frac{(|E_s|^2 - |E_f|^2)}{\lambda A_{eff}}. \tag{2}$$

Given the 20 nm spectrum tuning range, the n_2 varies minimally, allowing us to treat the factor $(2\pi L n_2/3)$ on the right-hand side as constant during the tuning process. Under the assumption that the overall phase difference ($\Delta\varphi$) remains constant throughout the wavelength tuning process, the factor $((|E_s|^2 - |E_f|^2)/\lambda A_{eff})$ should also remain constant. Given that A_{eff} is proportional to λ^2

[27], in our analysis, we consider λA_{eff} to be proportional to λ^3. Therefore, a reduction in pump power leads to a decrease in pulse peak power, subsequently causing a reduction in $(|E_s|^2 - |E_f|^2)$. This in return, results in a corresponding decrease in λ, ensuring the factor $\Delta\varphi$ remains consistent throughout the tuning process. This mechanism likely accounts for the phenomenon observed in the experiment, where the reduced pump power correlates with a blueshift of the center wavelengths.

Figure 4 shows the simulated overall phase difference at various pulse peak powers. The key parameters include a splicing angle of 30°, and a fiber length of 42 m. The nonlinear parameter γ *is* treated as inversely proportional to λ^3, set at $2\,W^{-1}km^{-1}$ at 1.55 µm [21]. To reflect experimental conditions, the simulation's pulse peak powers are set near the experimental values at the initial and end wavelengths in the tuning process, being 145 and 140 W, respectively, and includes an additional setting of 135 W for demonstration. The λ_1 corresponds to the initial experimental wavelength at 1588.9 nm, and the optimal phase difference (red dashed line) in the simulation is determined at this wavelength when the peak power is 145 W. Under the assumption that a consistent phase difference ($\Delta\varphi$) is kept between the original and new wavelengths during the tuning, the simulation yields a 19.5 nm tuning range. This is calculated by λ_1 minus λ_2 as the pulse peak power decreases from 145 to 140 W, closely approximating the 20.7 nm tuning range observed in the experiment. The center wavelength shifts from λ_1 to λ_3 as the pulse peak power reduces from 145 to 135 W, clearly indicating a blueshift trend in the center wavelength as the pulse peak power decreases. Given the NPE effect's key role in tuning, our findings could extend to NPE-based lasers across multiple wavelength bands.

In summary, we present the first L-band MLFL with an all-PM, all-fiber setup, achieving over 20 nm tuning range (1568.2 to 1588.9 nm) by adjusting the pump power between 45 and 115 mW. Our work marks the first wavelength tuning in the all-PM configured NPE lasers, indicating adaptability across various wavelength bands. Contrary to traditional methods reliant on optical filters, loss control or birefringence adjustment, our all-PM, all-fiber laser utilizes the pump-power-controlled method, avoiding mechanical or thermal adjustments for a robust, reliable, and cost-effective wavelength tuning.

Funding. Japan Society for the Promotion of Science (18H05238, 22H00209, 23H00174); Core Research for Evolutional Science and Technology (JPMJCR1872).

Acknowledgment. Sze Yun Set thanks Mr. Hideru Sato for the personal donation partially supporting this research work.

Disclosures. A US provisional patent application related to the work presented in this paper has been filed.

Data availability. Data underlying the results presented in this paper are not publicly available at this time but may be obtained from the authors upon reasonable request.

REFERENCES

1. C. W. Freudiger, W. Min, B. G. Saar, *et al.*, Science **322**, 1857 (2008).
2. S. Yamashita and Y. Takubo, Photonic Sens. **3**, 320 (2013).
3. Y. Cao, L. Wang, Z. Lu, *et al.*, Opt. Express **27**, 7988 (2019).
4. J. Jiang, Q. Huang, Y. Ma, *et al.*, Opt. Express **29**, 26332 (2021).
5. N. Nishizawa, Y. Chen, P. Hsiung, *et al.*, *Conference on Lasers and Electro-Optics* (Optica Publishing Group, 2004), paperCTuBB3.
6. Y. Ozeki and D. Tashiro, Opt. Express **23**, 15186 (2015).
7. M. Hofer, M. E. Fermann, A. Galvanauskas, *et al.*, Opt. Lett. **23**, 1840 (1998).
8. P. F. Curley, A. I. Ferguson, J. G. White, *et al.*, Opt. Quantum Electron. **24**, 851 (1992).
9. F. Huang, J. Si, T. Chen, *et al.*, IEEE Photonics Technol. Lett. **32**, 1025 (2020).
10. T. Zhu, Z. Wang, D. N. Wang, *et al.*, Photonics Res. **7**, 853 (2019).
11. J. L. Luo, L. Li, Y. Q. Ge, *et al.*, IEEE Photonics Technol. Lett. **26**, 2438 (2014).
12. J. Kang, C. Kong, P. Feng, *et al.*, IEEE Photonics Technol. Lett. **30**, 311 (2018).
13. X. Sun, Y. Zhu, L. Jin, *et al.*, Opt. Lett. **47**, 4913 (2022).
14. M. Dai, B. Liu, T. Shirahata, *et al.*, Opt. Express **31**, 27810 (2023).
15. H. Zhang, H. Xia, M. Fan, *et al.*, Photonics **10**, 184 (2023).
16. J. Szczepanek, T. M. Kardaś, C. Radzewicz, *et al.*, Opt. Lett. **42**, 575 (2017).
17. G. Ye, K. K. Chow, B. Liu, *et al.*, Opt. Lett. **48**, 4729 (2023).
18. X. Liu, Q. Li, D. Pan, *et al.*, J. Lightwave Technol. **39**, 1 (2021).
19. J. Szczepanek, T. M. Kardaś, C. Radzewicz, *et al.*, Opt. Express **26**, 13590 (2018).
20. Z. Peng, Z. Cheng, X. Bu, *et al.*, IEEE Photonics Technol. Lett. **30**, 2111 (2018).
21. G. P. Agrawal, *Nonlinear Fiber Optics*, 5th ed. (Elsevier/Academic, 2013).
22. S. F. Lin and G. R. Lin, Opt. Express **22**, 22121 (2014).
23. G. Ye, K.K. Chow, M. Dai, *et al.*, *2023 Asia Communications and Photonics Conference/2023 International Photonics and Optoelectronics Meetings (ACP/POEM)* (IEEE, 2023), p. 1.
24. Z. Wang, L. Zhan, X. Fang, *et al.*, J. Lightwave Technol. **34**, 4128 (2016).
25. P. M. Becker, A. A. Olsson, and J. R. Simpson, *Erbium-Doped Fiber Amplifiers: Fundamentals and Technology* (Elsevier, 1999).
26. J. Zhou, W. Pan, X. Gu, *et al.*, Opt. Express **26**, 4166 (2018).
27. B. D. Guenther and B. Steel, eds., *Encyclopedia of Modern Optics* 2nd ed. (Academic Press, 2018).